Wesleyan University

Big Disk Energy

by

Jonas Powell
Class of 2019

A thesis submitted to the
faculty of Wesleyan University
in partial fulfillment of the requirements for the
Degree of Master of Arts

Middletown, Connecticut April, 2018

If people sat outside and looked at the stars each night,

I'll bet they'd live a lot differently.

—Calvin & Hobbes

Acknowlegdments

Thanks!

Contents

Chapter 1

Introduction

Circumstellar disks of gas and dust, left over from the processes of stellar formation, are cosmic nurseries for the growth of planets. In these young stellar systems, bodies ranging from small and rocky to massive and gaseous coalesce as gravitational, chemical, and viscous evolution transform gas-rich protoplanetary disks into tenuous, nearly gas-free debris disks over millions of years. While the direct observation of planets during this stage is effectively impossible with our current technology, observations of emission from rotational transitions of gas species, scattered light from micron-sized dust grains, and thermal emission from micron to millimeter sized grains provide an indispensable tracer of the processes that shape these disks. Because the genesis of planets is directly tied to the morphology of the gas and dust, studying the anatomy of a variety of young disks is essential to understanding how worlds such as our own formed. 49 Ceti, at an estimated age of 40 million years, is just one puzzle piece of many, but its gas-rich debris disk provides important clues to deciphering the final stages of disk evolution.

Circumstellar disks, the remnants of the stellar formation process, are the birthplace of planetary systems. It is here that the primordial ingredients of stellar formation evolve over millions of years, starting as a thick, gas rich protoplanetary disk before thinning out to a rockier, dustier debris disk. Indeed, this is a familiar

story for us here on Earth, as the Solar System - our own local debris disk - underwent a similar transformation four and a half billion years ago as our Sun, then just a juvenile protostar, formed out of its stellar nursery. But while parts of this history lesson - our Genesis story - are well understood, others still present significant uncertainties. By observing and understanding other protostars and circumstellar disks, we are given the chance to walk back through time and see just how we got to where we are today.

1.0.1 Circumstellar Disk Formation and Evolution

Stars form when large molecular clouds develop a gravitational instability sufficient to lead to a runaway collapse process (reference). As the local material begins to self-gravitate, its center forms a dense core which will eventually become a young star (binaries are also common; are they more likely in HMSFRs?). However, the collapse also leads - almost inevitably (citation) - to a circumstellar disk, needed to shed angular momentum from the protostar, usually with mass around 0.5 % $M_{]odot}$. Since these disks form directly out of the collapse process, they (like their stellar host and the initial molecular cloud) are composed almost exclusively of H_2. $In these early stages, gas outweighs dust by around two orders of magnitude$

1.1 Summary of Contents

This thesis will primarily deal with...

Chapter 2

Observations

The data presented in this thesis are part of an ALMA survey of Orion proplyds in Orion (project 2011.0.00028.S); data collection and analysis methods of the continuum results are presented in (Mann et al. 2014). Since this was part of a Cycle 0 Early Science project, the survey used only 22 of the array's 12 meter dishes in a hybrid configuration, with baselines ranging from 21.2 to 384.2 meters, yielding maximum angular scales and angular resolution of 8" and 0."5, respectively. At a distance of 389 pc for the distance to these sources, max angular scales and angular resolution correspond to 3,112 AU and 194 AU, respectively. The distance to the stars used here was recently measured by GAIA ((Collaboration 2016), (Collaboration et al. 2018)) to be 389 $\pm 7.97, nearer than the previous measurement of 414 pc.$

Observations were made in Band 7 in four 1.875 GHz-wide bands arranged to cover the rest frequencies of the HCO+ (4-3), HCN (4-3), CO (3-2), and CS (7-6) transitions (356.734 GHz, 354.505 GHz, 345.796 GHz, and 342.883 GHz, respectively). Each band was split into 3840 channels with width 488.28 kHz, yielding a velocity resolution of 0.42 km s^{-1}.

Analysis showed that excluding baselines shorter than 110 kλ, 80 kλ, and 60 kλ for HCO^{+1}, HCN, and CO respectively optimized signal-to-noise ratios for each data set. The CS line showed no improvement with baseline cutting. These cuts resulted in decreased maximum recoverable angular scales of 1, 2, and 3.

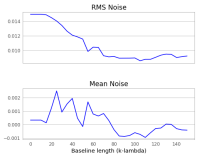

Figure 2.1: A figure

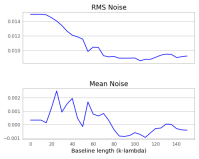

Figure 2.2: Another figure

The data presented here, from Field 4 of Mann et al (2014) (citation) represent 13.6 minutes of on-source time. This duration was split into six 136 second observations, spaced out over 7.5 hours to ensure adequate *uv* coverage, resulting in a synthesized beam of 0.”57 0.”51 with a position angle of PA. Precipitable water vapor in the atmosphere was stable at 0.7 mm.

The data were calibrated by ALMA staff using standard procedures in the Common Astronomy Software Applications (CASA, citation). The antenna-based complex gains and bandpass response of the system were calibrated using observations of the quasars J0607-085 and J0522-364 respectively. The ab- solute flux calibration was determined from observations of Callisto. The model of Callisto was drawn from Butler (2012) (citation). Absolute flux calibration is estimated to be accurate to within 10% (Mann et al. 2014).

The velocity reference frame was converted from CASA’s standard topocentric frame to LSRK (kinematic local standard of rest) using the CASA task cvel. Next, continuum emission was subtracted in the uv plane using the CASA task contsub. Visibilities were then inverted with natural weighting, deconvolved, and restored using standard procedures from the Multichannel Image Reconstruction Image Analysis and Display, or MIRIAD, package (Sault et al. 1995) (citation)

Chapter 3

Results

3.1 Modeling

Spatially and spectrally resolved line emission was detected for CO (3-2), HCO^+ (4-3), HCN (4-3), and CS (7-6) across around 50 channels of width 0.42 km s^{-1}. Detailed studies of gas structure in protoplanetary disks are still relatively rare, and have previously only focused on disks in nearby low-mass star-forming regions (SFRs). Consequently, it would be useful to develop a rough understanding of the observations before beginning detailed modeling. This includes removing cloud contamination, investigating the general morphology of the disks using moment maps, estimating the disks' gas masses using integrated line flux, and examining the velocity profile to estimate the mass of the central star (really?).

Cloud contamination occurs when emission from background or foreground gas clouds is detected in the same direction as the disk being observed. Since the Orion Nebula has a higher gas density than in low-mass SFRs, cloud contamination is more much common and problematic. "Previous observations of these disks by Mann Williams (2009) (citation) (do I have these?) strongly detected the CO (3-2 line)". Thanks to the higher sensitivity of the ALMA observations, etc.

CO displayed the most significant cloud contamination, thanks to its low critical density and higher abundance in the clouds. For the other molecular lines,

which have higher critical densities, cloud contamination is less severe but still clearly present in HCO^+, which is the brightest tracer.

Since cloud contamination inherently tends to be large-scale in structure, excluding short baselines reduces its contribution to the observations. While this process slightly reduces the total recovered flux from the disk and our ability to characterize its large-scale strucutre, it is necessary to avoid including cloud emission from the cloud in the process of fitting the disk emission. By evaluating mean and RMS noise for an off-source region of the field while varying the minimum baseline used, we found that excluding baselines less than 110 kλ, 80 kλ, and 60 kλ for HCO^+, HCN, and CO, respectively, yielded optimum results. Since the CS line already has a very low SNR and a higher critical density, excluding baselines did not improve the observations.

Table 1: Integrated Flux Measurements Line — Baselines — Max Angular Scale — Integrated Line Flux (Jy km s^{-1}) CS (7-6) All CO (3-2) All CO (3-2) >60 kλ HCN (4-3) All HCN (4-3) >80 kλ HCO^+ All HCO^+ >110 kλ

Figure 1:

The effects of these exclusions are detailed in Table 1 and demonstrated on the HCO^+ line in Figure 1. (Analysis of these plots, bottom of p.3 in Factor et al)

In all lines, rotation of each disk is clearly visible as a transition from red-shifted emission in one corner to blue-shifted emission in the other corner***. The maximum extent of the 3-σ contours along the disks' major axes correspond to outer diameters of the HCO+ disks of A and B; outer diameters of the HCN disks of A and B; and outer diameters of the CO disks of A and B, all at a distance of 389pc. The CS emission is not detected strongly enough to provide a reliable measurement (check that this is true)

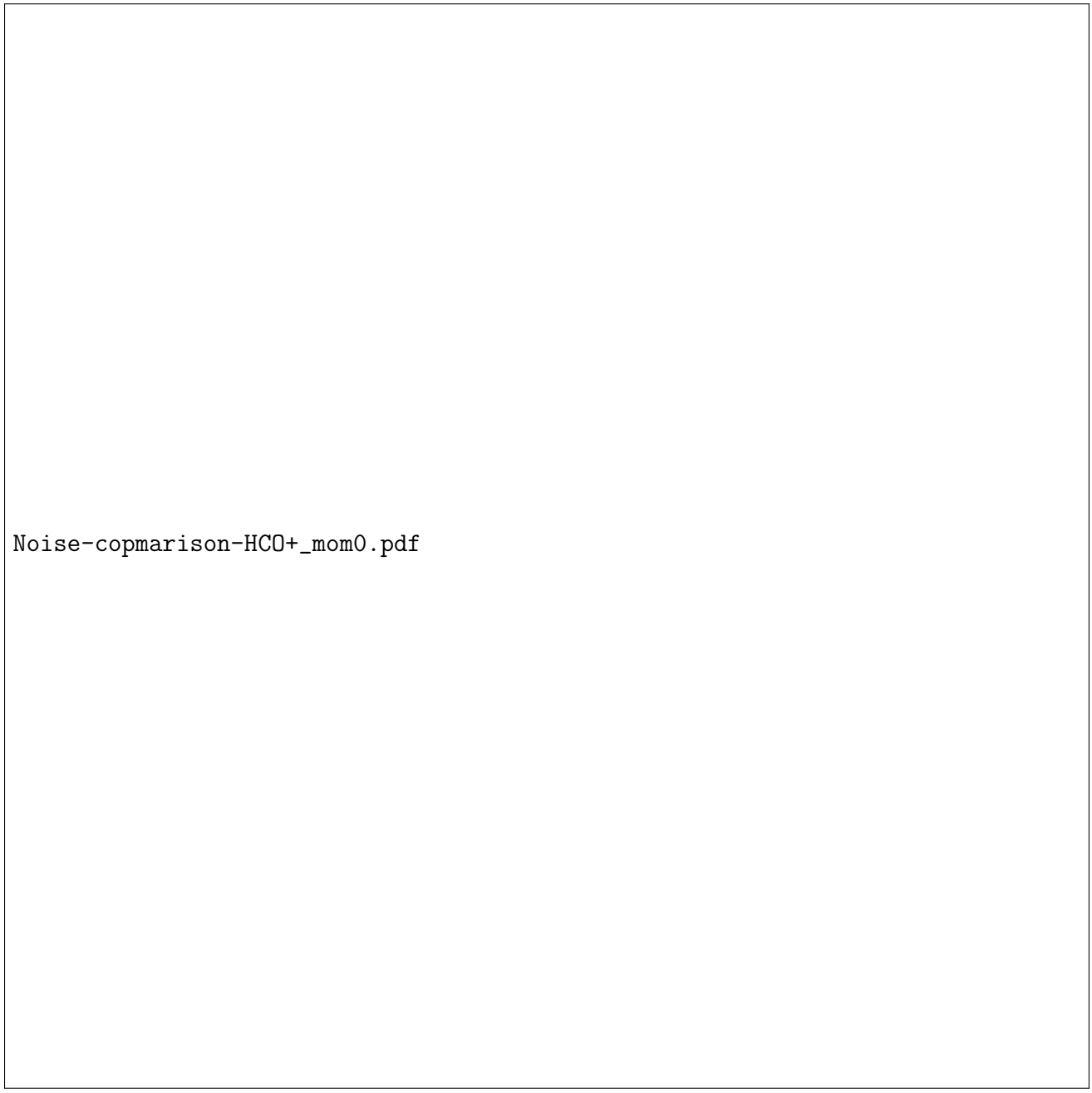

Figure 3.1: blah

Tables 2 and 3 present the velocity-integrated line fluxes and the best-fit parameters for a simple elliptical Gaussian fit to the visibilities for each disk, respectively. Integrated line flux was measured using the MIRIAD task cgcurs to integrate the intensity in the zeroth-moment map throughout the region enclosed by the 3 σ contour level. Uncertainties in the integrated line flux do not include the 10% absolute flux calibration uncertainty inherent in the ALMA observations caused by uncertainties int he models of solar system objects used as flux callibrators. Elliptical Gaussian fits of the visibilities were performed using the MIRIAD task uvfit.

Assuming optically thin emission (maybe good?) and Local Thermodynamic Equilibrium (LTE), the line-emitting gas mass, $\mathrm{M_{gas}}$ is given by:

$$M_{\mathrm{gas}} = \frac{4\pi}{h\nu_0}\frac{Fmd^2}{A_{ul}X_u}, \tag{3.1}$$

where F is the integrated line flux, m is the mass of the emitting gas molecule, d is the distance to the source, h is the Planck constant, ν_0 is the molecular line's rest frequency, A_{ul} is the Einstein coefficient for the $(u-l)$ transition, and

$$X_u = \frac{N_u}{N_{\mathrm{tot}}} = (2J_u+1)\frac{\exp[-B_0 J_u(J_u+1)hc/kT_{\mathrm{ex}}]}{kT_{\mathrm{ex}}/hcB_0}. \tag{3.2}$$

In (2), $\frac{N_u}{N_{\mathrm{tot}}}$ is the ratio of the number of molecules in the upper state to the total number of molecules; J_u is the quantum number of the upper level; B_0 is the rotation constant in units of wavenumber; h and c are the Planck constant and speed of light, respectively; and T_{ex} is the excitation temperature. VALUES FOR

$A_U LAND B0 WERE TAKEN FROM MOLECULAR DATA MADE AVAILABLE BY SHOIER$

A position-velocity diagram for HCO^+ is shown in Figure 4, showing the position, as a function of velocity, of emission form a cut along the major axis of the disk (FIGURE OUT HOW TO DO THIS). ANALYSIS of this stuff.

To find best fit values, we use disk modeling and ray-tracing code developed by **?**. The code turns a set of paramters describing the disk's physical structure (atmospheric temperature, density structure, molecular abundances, and so on) into a three dimensional model. Given observational characteristics (distance, inclination, and so on), it can then turn that model into a simulated sky-projected image which may then be compared to our observational data.

Explorations of paramter space were implemented through

Things to get: * Rewrite this whole thing. * Previous observation of these disks with SMA? Maybe Mann Williams 2009. What did they detect? * Integrated Flux Measurements * Make a 2-image subplot of HCO+ with and without baseline cutting. Moment 0 or Moment 1? Show n-sigma contours * Find max width of disks for each line by 3-sigma contour

* Make moment0 and moment1 plotters. Two panel or just 1? Should have contouring. * Use cgcurs to get integrated line flux in moment0 map. * use uvfit for elliptical guassian vis fits. * PV Diagram * Gas mass calculations

Chapter 4

Results

4.1 Reduction Strategies

Chapter 5

Results

5.1 Reduction Strategies

Chapter 6

Conclusion

6.1 Something

6.2 Future Work

6.3 Prospects of the field

6.4 Acknowledgments

This work has made use of data from the European Space Agency (ESA) mission *Gaia* (`https://www.cosmos.esa.int/gaia`), processed by the *Gaia* Data Processing and Analysis Consortium (DPAC, `https://www.cosmos.esa.int/web/gaia/dpac/consortium`). Funding for the DPAC has been provided by national institutions, in particular the institutions participating in the *Gaia* Multilateral Agreement.

Bibliography

Collaboration, G. 2016, Astronomy & Astrophysics, 595, A1, arXiv: 1609.04153

Collaboration, G., Brown, A. G. A., Vallenari, A., Prusti, T., de Bruijne, J. H. J., Babusiaux, C., & Bailer-Jones, C. A. L. 2018, Astronomy & Astrophysics, 616, A1, arXiv: 1804.09365

Factor, S. M., et al. 2017, The Astronomical Journal, 153, 233, arXiv: 1704.01970

Goodman, J., & Weare, J. 2010, Communications in Applied Mathematics and Computational Science, 5, 65

Mann, R. K., et al. 2014, The Astrophysical Journal, 784, 82, arXiv: 1403.2026

Mann, R. K., & Williams, J. P. 2009, The Astrophysical Journal, 699, L55

Ricci, L., Robberto, M., & Soderblom, D. R. 2008, The Astronomical Journal, 136, 2136

Ricci, L., Testi, L., Williams, J. P., Mann, R. K., & Birnstiel, T. 2011, The Astrophysical Journal, 739, L8

Smith, N., Bally, J., Licht, D., & Walawender, J. 2005, The Astronomical Journal, 129, 382

Williams, J. P., et al. 2014, The Astrophysical Journal, 796, 120, arXiv: 1410.3570